Robustness of Ensemble Deep Learning Model with Zebra Optimization Algorithm for Weather-Related Disaster Detection System Using Remote Sensing Images

Daniel Arockiam[1,2,*] , Azween Abdullah[3], Valliappan Raju[4]

[1]Postdoctoral Fellow, Perdana University, Kuala Lumpur 50490, Malaysia

[2]Amity University Madhya Pradesh, Gwalior 474005, India

[3]Faculty of Applied Science and Technology, Perdana University, Kuala Lumpur 50490, Malaysia

[4]Open & Dist. Learning Centre, Perdana University, Kuala Lumpur 50490, Malaysia

Emails: daniel.arockiam@perdanauniversity.edu.my; azween@perdanauniversity.edu.my; valliappan@perdanauniversity.edu.my

Abstract

Weather monitoring is a vital challenge in dissimilar areas of applications such as military missions, higher precision agriculture, outdoor entertainment and recreation, industrial manufacture, and logistics. The most vital application is natural weather disaster monitoring. Weather change has made stronger an occurrence of natural disasters all over the world. More extreme climate events have been experienced for the past few years, like lower and higher temperatures, sturdy winds in humid cyclones, heavy rains, and intensified lack. Therefore, at present, remote sensing imagery (RSI) analysis is necessary in the field of ecological and weather monitoring mainly for the application of identifying and handling a natural climate disaster. To upsurge the accuracy of detection, machine learning (ML) and deep learning (DL) systems were applied to enhance the efficacy of removing features and help to perceive large-scale losses like landslides, earthquakes, and floods. In this manuscript, we design and develop a Weather Disaster Detection Model Using Zebra Optimization Algorithm with Ensemble Learning on Remote Sensing Images (WDDZOA-ELRSI) technique. The proposed WDDZOA-ELRSI model's main intention is to improve the detection model of weather disasters using state-of-the-art DL methods. Initially, the bilateral filter (BF) method is employed in the image pre-processing stage to eliminate the unwanted noise from input data. Furthermore, the feature extraction method executes GoogleNet technique to transform raw data into a reduced set of relevant features. For the classification process, the ensemble of deep learning models such as conditional variational autoencoder (CVAE), graph convolutional network (GCN), and Elman recurrent neural network (ERNN) have been deployed. Eventually, the zebra optimization algorithm (ZOA)-based hyperparameter tuning procedure has been achieved to improve the detection outcomes of ensemble models. The simulation analysis of the WDDZOA-ELRSI system is verified on a benchmark image dataset and the outcomes were evaluated under numerous measures. The simulation outcome emphasized the enhancement of the WDDZOA-ELRSI model in the weather disaster detection process

Keywords: Weather Related Disaster Detection; Zebra Optimization Algorithm; Ensemble Learning Model; Remote Sensing Images; Feature Extraction

1. Introduction

Weather monitoring is a major challenge in diverse fields of applications, for example, outdoor entertainment, logistics, higher precision agriculture, military missions, industrial recreation, and production [1]. One of the crucial applications is natural disaster monitoring. Climate change has strengthened the existence of natural disasters globally. More fervent weather events became skilled in the past several decades, like heavy rains, lower and higher temperatures, intensified droughts, and strong winds in tropical cyclones [2]. People can be susceptible to the significance of extreme weather events, for instance, river overflow, coastal erosion, flash flooding in

DOI: https://doi.org/10.54216/FPA.190117
Received: October 14, 2024 Revised: January 03, 2025 Accepted: February 02, 2025

underground drainage galleries, soil, landslides on slopes, and infrastructural collapsing of buildings and houses [3]. Moreover, human loss and climate-related natural disaster events affect the local economy by destroying productive capital, housing stock, and supply chain. Disaster management performs a vital role during urban planning for social and economic progression [4]. For such planning, near real-world disaster evaluation maps through change recognition are crucial for immediate responsive event management.

Nowadays disaster recognition is one of the active fields of investigation in remote sensing (RS) because saving human life is our priority once a disaster arises [5]. It is vital in the coordination of faster responsive actions after a destructive disaster like flood or landslide. While, floods are represented by a massive water flow in huge magnitudes into dry lands from water bodies like rivers, oceans, and lakes [6]. Usually, the water level change in the water bodies is distantly monitored, specifically in emerging countries, and frequently neglected until it outcomes in flood-related disasters [7]. In addition, floods are the most commonly arising natural disasters worldwide. Flood maps are developed to retrieve data from satellite imagery, aircraft, RS models, or UAVs [8]. The image data taken by satellite can aid in implementing appropriate risk assessments of affected fields to bring about appropriate disaster response. RS is a productive method as it decreases search endeavours and offers an instant rescue source [9]. The Incorporation of GIS and RS imagery for disaster management methods has assured to time- and cost-effective device for distributing critical decisions and information. To raise the recognition accuracy, deep learning (DL) and machine learning (ML) are applied to enhance the efficacy of removing features [10]. An extensive number of novel reports on recognition depend on DL and ML to identify large-scale damage.

This manuscript designs and develops a Weather Disaster Detection Model Using a Zebra Optimization Algorithm with Ensemble Learning on Remote Sensing Images (WDDZOA-ELRSI) technique. Initially, the bilateral filter (BF) method is employed in the image pre-processing stage to eliminate the unwanted noise. Furthermore, the feature extraction method executes the GoogleNet technique. For the classification process, the ensemble of DL models such as conditional variational autoencoder (CVAE), graph convolutional network (GCN), and Elman recurrent neural network (ERNN) have been deployed. Eventually, the zebra optimization algorithm (ZOA)-based hyperparameter tuning procedure has been achieved to improve the detection outcomes of ensemble models. The simulation analysis of the WDDZOA-ELRSI system is verified on benchmark image dataset and the outcomes were evaluated under numerous measures.

2. Literature Review

In [11], a Big Data Set-based PICA method is presented for applying an image-processing model, identifying disaster, and assessing outcomes with PICA assistance that permits examination of disaster to remove more effectually. The presented method makes adjustments and tailoring acquired from satellite images before training and post-disaster aerial image patching data. Shastry et al. [12] developed a semantic labeled database of higher-resolution multi-spectral images strategically sampled for representation of North American surface water changeability along 5 spatiotemporal levels: topographic complexity, latitude, day of year, and land use. These databases are employed to train a CNN to automatically identify inundation extents utilizing the DELTA structure an open-source TensorFlow or Keras interpreter for satellite imagery. Sarkar et al. [13] aimed to implement and introduce the VQA structure for post-disaster damage assessment depending upon drone imagery such as SAM-VQA. In VQA, query-based answers from images in terms of situations in disaster-affected regions can deliver significant data to make decisions.

Roohi et al. [14] handle this gap by incorporating AI, geospatial data, RS, and to recognize flood-affected regions. It implements DL models, particularly FCN and U-Net models, to radar and optical images from 4 flood events. Hamza et al. [15] projected an innovative bottleneck residual and self-attention fusion-assisted structure for recognition of land use from RS images. Initially, it projects to employ the faster neural model to create cloud-effect satellite images. Then, features were removed from the deep layers and combined by utilizing a novel serial method depending on weighted entropy. By extracting superfluous and redundant data, an innovative chimp optimizer model is implemented to the fused aspects and refined them. Finally, selected aspects are categorized utilizing the assistance of NN classifiers.

Paul and Janani [16] introduce a progressive disaster mitigation and weather monitoring method that integrates flood zone detection, interactive weather visualizations, emergency shelter mapping, and unplanned drainage identification. The projected method provides optional drought intensity prediction ability. The objective of this method is to deliver accurate and timely data to aid communities prepare and responding to weather-related emergencies. Flood zone recognition employs satellite imagery and data analysis models to recognize fields at risk of flooding, allowing authorities to evacuate residents and timely warnings if needed. The unplanned drainage recognition aspects employ ML models to monitor and detect the region's absence of proper drainage methods, allowing authorities to take proactive measures to preclude flood damage. Ge et al. [17] developed an incremental learning structure for quick recognition of collapsed buildings caused by sudden natural disasters. Particularly, end-to-end gradient boosting systems are enhanced to an incremental learning structure for an emergency response.

DOI: https://doi.org/10.54216/FPA.190117
Received: October 14, 2024 Revised: January 03, 2025 Accepted: February 02, 2025

3. Proposed Methodology

In this manuscript, we design and develop a WDDZOA-ELRSI technique. The proposed WDDZOA-ELRSI methodology main intention is to improve the detection model of weather disasters using state-of-the-art DL methods. It contains distinct kinds of stages involved as image preprocessing, feature extractor, ensemble classification model, and parameter selection. Fig. 1 portrays the workflow of the WDDZOA-ELRSI technique.

A. Image Preprocessing

Initially, the BF method is employed in the image pre-processing stage to eliminate the unwanted noise from input data. Image pre-processing is applied to improve image quality and reduce noise in the input images [18]. Now, an input image K_r is given as input to the bilateral filter (BF) and a preprocessed image K_a is achieved. A BF is considered a nonlinear filter, which relies on local image information. Besides, the image's pixel value and spatial location information are measured utilizing BF to protect the image edges throughout the denoising process. Furthermore, a BF uses a weighted average of the neighbourhood to replace all noise pixels and is computed as,

$$b(l) = \frac{1}{c_e}\sum_{d\in\Omega} c_f\,(l,d)c_g(l,d)A(d) \tag{1}$$

Whereas $b(l)$ characterizes the filter's output pixel value, $A(d)$ signifies the pixels in the new input image, Ω identifies the vicinity of the pixel l, c_e specifies normalization factor and is computed as, $c_e = \sum_{d\in\Omega} c_f\,(l,d)c_g(l,d)$, c_f represents the spatial kernel and is stated as $c_f = exp\left[-\frac{|l-d|^2}{\sigma_f^2}\right]$, c_g signifies range kernel and is stated as $c_g = exp\left[-\frac{|A(l)-A(d)|^2}{\sigma_g^2}\right]$ σ_f and σ_g are denotes smoothening parameters.

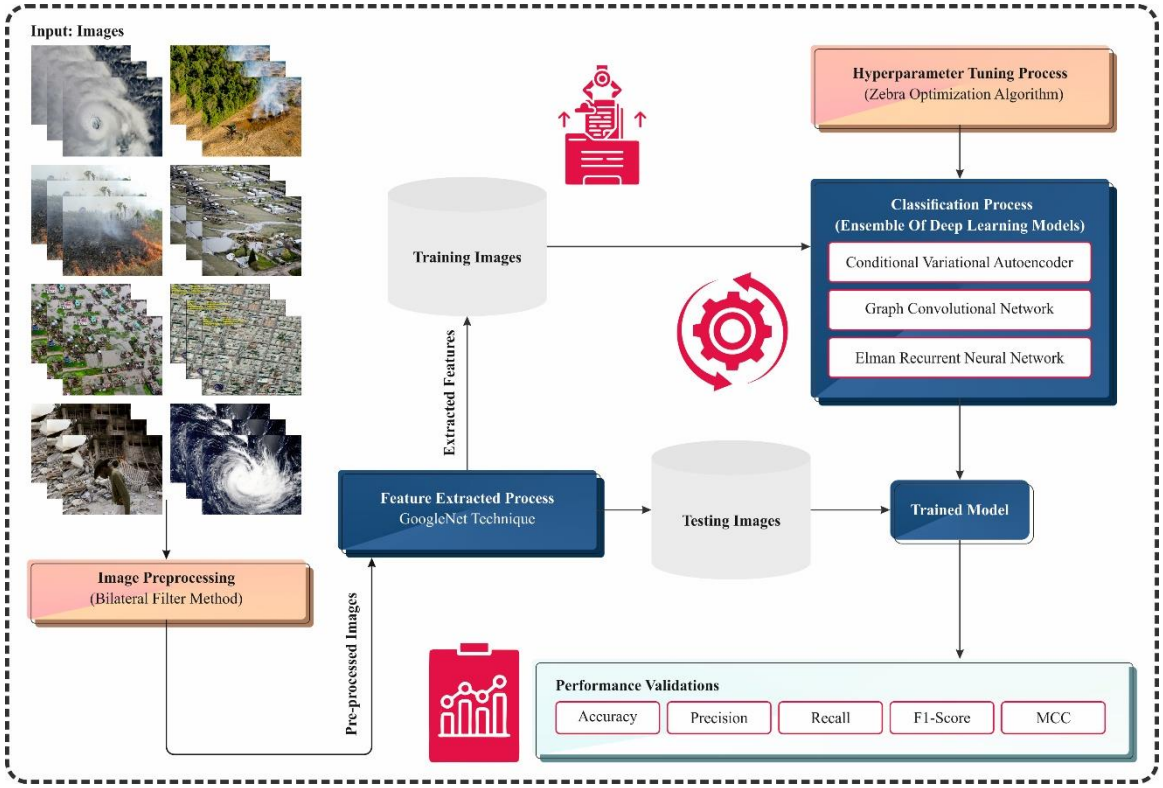

Figure 1. Workflow of WDDZOA-ELRSI technique

B. Feature Extraction

Furthermore, the feature extraction method executes GoogleNet technique to transform raw data into a reduced set of relevant features. The GoogLeNet module is extensively applied for feature extraction from user's data because of its inception module that achieves learning features at dissimilar scales utilizing 1x1, 3x3, and 5x5 convolutions [19]. The normal application framework of the inception module comprises 22 parameterized layers of fully connected and convolutional layers. By combining non-parameterized pooling layers, the layer counts in the GoogLeNet method attain 27. The primary goal of the inception module is to decrease the parameter counts in deeper methods while preserving networking depth and presenting a sparse network structure rather than a dense structure. Compared to AlexNet, which has 60 million parameters, GoogLeNet has only four million parameters

DOI: https://doi.org/10.54216/FPA.190117
Received: October 14, 2024 Revised: January 03, 2025 Accepted: February 02, 2025

and contains a considerably deep framework. GoogLeNet includes nine identical inception units, using 3 dissimilar convolution processes for feature extraction. In addition, an additional 1x1 convolution layer is incorporated in the inception layer for reducing the dimensions, together with a parallel max-pooling layer. The outputs of each of the convolution layers are concatenated for last of the inception layers to connect to the following module.

The hidden state of GoogLeNet is calculated utilizing Eq. (2).

$$H_t = Dropout\left(Flatten\left(concat(conv1, conv3, conv5)\right)\right) \quad (2)$$

After concatenation, the fattened layer has been used together with dropout. The hidden representation is calculated and given to the last dense layer of the GoogLeNet module as shown.

$$Dense_{GoogLeNet} = (W * H_t + b) \quad (3)$$

This last dense layer of GoogLeNet, after learning the features, is then given to the hybrid module to be concatenated with the last dense layer of ResNet.

C. Ensemble Disaster Classification Model

For the classification process, an ensemble of DL models such as CVAE, GCN, and ERNN models have been deployed.

i) CVAE Model

The CVAE model is used, in this paper, containing dual encoders signified as r_1 and q, and a decoder represented as r_2 [20]. The strain data d_i and the equivalent GW initial parameters θ_i from the $i\ th$ sample of the dataset are connected to the encoder q. Then, the encoder q makes the standard deviation σ_q and mean μ_q to build a normal distribution $N(\mu_q, \sigma_q)$ for the latent variable z. Sampling is then implemented from the distribution $N(\mu_q, \sigma_q)$ to make $z_{samples}$. All $z_j \in z_{samples}$ is input to the decoder r_2 together with d_i, leading to the standard deviation $\sigma_{r_2}(Z)$ and mean $\mu_{r_2}(Z)$ to build a normal distribution $N\left(\mu_{r_2}(z_j), \sigma_{r_2}(Z)\right)$ of θ'. By incorporating each normal distribution consistent to $z_{samples}$, a complex distribution is built to estimate the Bayesian posterior distribution $p(\theta|d_i)$. Nevertheless, this procedure needs the input to include θ_i, which isn't accessible after testing d_i with unidentified θ_i. Fig. 2 depicts the infrastructure of CVAE.

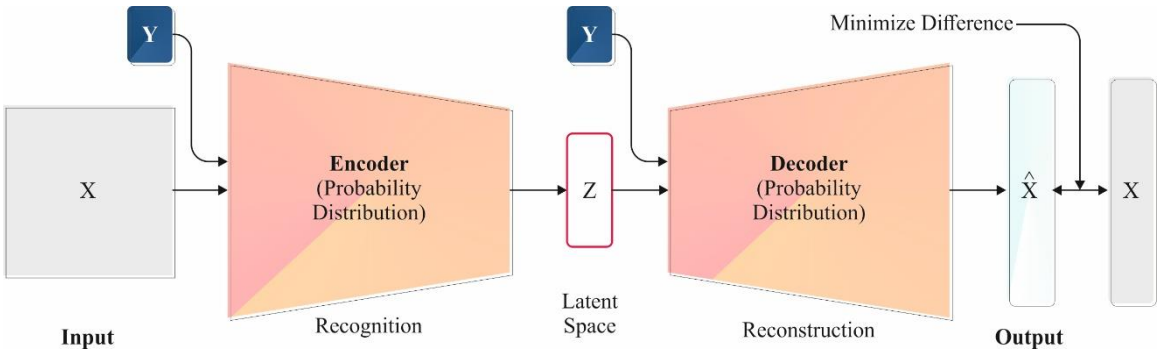

Figure 2. CVAE Architecture

To deal with this problem, the method presents the encoder r_1. By input only d_i into encoding r_1 to get the standard distribution $N(\mu_{r_1}, \sigma_{r_1})$ and training the model to reduce the discrepancy among $N(\mu_{r_1}, \sigma_{r_1})$ and $N(\mu_q, \sigma_q)$, encoder r_1 is applied in testing to make the distribution of the latent variable z rather than encoder q. The discrepancy between the distribution $q\phi(z|\theta_i, d_i) \equiv N(\mu_q, \sigma_q)$and the distribution $r_{\rho_1}(z|d_i) \equiv N(\mu_{r_1}, \sigma_{r_1})$ is evaluated utilizing the Kullback-Leibler (KL) divergence D_{KL} among the dual distributions, described as

$$D_{KL}\left(q\phi(z|\theta_i, d_i) r_{p1}(Z|d_i)\right) \equiv \int d\,z q\phi(z|\theta_i, d_i) log\left[\frac{q\phi(z|\theta_i, d_i)}{r_{\rho_1}(z|d_i)}\right] \quad (4)$$

The discrepancy in the distribution $r_{\rho_2}(\theta'|z, d_i) = \frac{1}{n}\sum_j^n N\left(\mu_{r_2}(z_j), \sigma_{r_2}(Z)\right)$ and the true posterior $p(\theta|d_i)$ approximated by the method is assessed utilizing the loss of reconstruction $-E_{q\phi(z|\theta_i, d_i)}[\log r_{\rho_2}(\theta_i|z, d_i)]$. Now, the variable n indicates the total number of $z_{samples}$.

DOI: https://doi.org/10.54216/FPA.190117
Received: October 14, 2024 Revised: January 03, 2025 Accepted: February 02, 2025

In terms of the CVAE method, it is established that the sum of the reconstruction loss and KL divergence loss characterizes an upper boundary on the true loss of the approach.

ii) GCN Technique

GCNs are a kind of CNN, which straightforwardly operates on graph structures, utilizing the inherent relationships among nodes for efficient feature extraction from node data [21]. In comparison with conventional statistic models, GCNs are well qualified to seizure composite data patterns and dependencies. As a result, GCN is selected to remove spatial features and discover primary designs in crime data. After the implementation of GCN, the graph data is converted into a tensor. The computing operation is delineated by the following equations:

$$\tilde{A} = A + I \tag{5}$$

$$\widetilde{D} = \sum \tilde{A}_{ij}, \tag{6}$$

$$H^{l+1} = \sigma\left(\widetilde{D}^{-\frac{1}{2}}\tilde{A}\widetilde{D}^{-\frac{1}{2}}H^{l}\omega^{l}\right). \tag{7}$$

Whereas H^l signifies the input state at layer l, σ refers to activation function (normally the sigmoid function), A embodies the adjacency matrix, which encodes relations among nodes, ω^l characterizes the learnable weighting parameters at layer l, and D refers to diagonal degree matrix (frequently applied in the Laplacian matrix calculation).

iii) ERNN Classifier

Unlike traditional feed-forward networks, ERNN incorporates feedback loops, permitting it to preserve data from preceding frames and well understand the event sequences [22]. This makes ERNN efficient at discovering refined discrepancies or tampering through numerous frames. Moreover, ERNN might find complex designs in sequential data that are advantageous to identify forgeries, which possibly span numerous frames or include small modifications. In comparison with other methods, like CNNs that mainly focus on spatial characteristics, the ability of the ERNN to handle temporal relations offers different benefits in identifying.

This model achieves the chosen feature and models intrusions consuming them. During this ERNN method, the buffering layer is identified as the recurrent layer, which permits the outputs of the hidden layer (HL) to address themselves. It allows the feedback to be identified and learned, and provides temporal and spatial trends. Thus, the HL state including one over the previous is replicated within the recurrent layer. Accordingly, the recurrent neuron amounts correspond to the HL amounts. At last, the ERNN comprises a HL, a recurrent layer, an input, and an output, which gives layered data. All layers are presented in one or more neurons, and they use the calculation of a nonlinear function.

It comprises m and n neurons inside the input layer of the HL and a single output module. Assuming $x_{it}(i = 1,2, \dots, m)$ specifies the collection of neurons' input vector at $t\ th$ time. The networking output at time $t + 1$ is suggested by y_{t+1}, the HL neuron output at $t\ th$ time is restructured by $(0 = 1,2, \dots, n)$, and the neurons of the recurrent layer became described by $\left(r_{jt} = 1,2, \dots, n\right)$. Node i inside the neurons of input layer is related to node j within the HL by the weight named w_{ij}. The node is related to node j within the HL neurons and output by weights v_j and cj, correspondingly. However, inputs of each neuron in the HL are followed by:

$$net_{jt}(l) = \sum_{i=1}^{n} w_{ij}\, x_{ij}(l-1) + \sum_{j=1}^{m} c_j\, r_{jt}(l) \tag{8}$$

$$r_{jt}(l) = x_{jt}(l-1), i = 1,2, \dots, n, j = 1,2, \dots, m \tag{9}$$

In the hidden neuron's output:

$$x_{jt}(l) = f_H\left(net_{jt}(l)\right) = f_H\left(\sum_{i=1}^{n} w_{ij}\, x_{ij}(l) + \sum_{j=1}^{m} c_j\, r_{jt}(l)\right) \tag{10}$$

Now, the function of the activation $f_H(x) = 1/(1 + e - x)$ inside the HL is particular to the sigmoid. The stated by the HL output:

DOI: https://doi.org/10.54216/FPA.190117
Received: October 14, 2024 Revised: January 03, 2025 Accepted: February 02, 2025

$$y_{t+1}(l) = f_T\left(\sum_{j=1}^{m} v_j\, z_{jt}(l)\right) \tag{11}$$

Here, $f_T(x)$ represents the activation function and denotes individuality mapping.

The training stages comprise the main weighted initialization stages that capture different random data, transmit ERNN forward and reverse, and calculate new weights. The ERNN hyperparameter, learning rate, batch size, dropout rate, and comprising momentum, are selected based on the best solutions.

D. Hyperparameter Tuning using ZOA

Eventually, the ZOA-based hyperparameter tuning procedure has been achieved to improve the detection outcomes of ensemble models. The ZOA is a new swarm intelligence model, which draws inspiration from zebras' normal free-flowing behavior, particularly their defense strategies and feeding habits against predators [23]. Their fur that is striped in white and black differentiates zebras. These stripes either hide zebras from predators or give a defensive power against biting flies. These animals that can run faster owing to their long and thin legs, single-toed feet, and architecture appropriate for feeding on grasses near the ground, show dual basic conduct in their social life regarding defense and feeding approaches. In the feeding procedure, a resulting zebra directs the group and guarantees that they attain the pastures, whereas other zebras converge on a wide range in the influence of these pioneers. During defense tactics, zebras generally attempt to escape from predators by zigzagging. Sometimes, in particular cases, zebras work together as a group and target to scare or divert predators. These dual underlying behaviors became the major stimulation for the mathematical modeling of ZOA. Stimulated by these natural behaviors, ZOA efficiently balances exploitation and exploration, and imitations display that ZOA is more effective than other optimizer methods. The succeeding imitations of zebra behavior are applied to the mathematical modeling of ZOA.

All zebras in ZOA, a population-based optimizer approach, represent promising solutions. The plain while the zebras live is a depiction of the searching region of the issue. A matrix defines the complete population, then a vector characterizes all individual zebras. The zebra's location defines the decision variable values. The primary locations are randomly allocated, and the ZOA's population matrix is mathematically described in Eq. (12):

$$X = \begin{bmatrix} X_1 \\ \vdots \\ X_i \\ \vdots \\ X_n \end{bmatrix}_{N\times m} = \begin{bmatrix} x_{1,1} & \dots & x_{1,j} & \cdots & x_{1,m} \\ \vdots & & \vdots & & \vdots \\ x_{\mathrm{i},1} & \dots & x_{\mathrm{i},j} & \cdots & x_{i,m} \\ \vdots & & \vdots & & \vdots \\ x_{\mathrm{N},1} & \dots & x_{\mathrm{N},j} & \cdots & x_{\mathrm{N},m} \end{bmatrix} \tag{12}$$

Now, the zebra population is characterized by X, while X_i denote $i\ th$ zebra and x_{ij} represent $j\ th$ problem variable value presented by the $i\ th$ zebra. The zebra's population size is symbolized by N, whereas the decision variable number is represented by m. All zebras characterize a possible key for the optimizer subject. The values recommended by the zebras for the problem variables are applied after estimating the objective function, and a vector in Eq. (13) signifies the outcome of the objective function.

$$F = \begin{bmatrix} F_1 \\ \vdots \\ F_i \\ \vdots \\ F_N \end{bmatrix}_{N\times 1} = \begin{bmatrix} F(X_1) \\ \vdots \\ F(X_i) \\ \vdots \\ F(X_N) \end{bmatrix}_{N\times 1} \tag{13}$$

The candidate choice is established and the solution qualities are estimated utilizing the values of the objective function (F vector). The zebra with the minimal value is the best solution for the problem of minimization, while the zebra with the maximal value is the best solution for the problem of maximization. The zebra's locations and values are upgraded in all iterations. During this upgrade, the zebra's natural behaviours, foraging, and defence tactics, are applied. In this case, the ZOA population is upgraded in dual dissimilar phases in all iterations.

DOI: https://doi.org/10.54216/FPA.190117
Received: October 14, 2024 Revised: January 03, 2025 Accepted: February 02, 2025

1) FORAGING

In the first stage of ZOA, the population is modernized by mimicking the feeding habits of zebra. Zebras generally eat grasses, and the plains zebra eat longer, non-nutritious grasses, permitting other species to access shorter grasses. The best candidate for ZOA is referred to as the pioneer zebra" and guides the others. Eqs. (14)−(16) Demonstrate how the pioneer zebra directs other candidates to its position in the searching region:

$$x_{i,j}^{t+1} = x_{i,j} + r \cdot \left(PZ_j - l \cdot x_{i,j}^{t}\right) \tag{14}$$

$$l = round(1 + rand) \tag{15}$$

$$X_i^t = \begin{Bmatrix} X_i^{t+1} & if(F_i^{\tau+1} < F_i^{\tau})_t \cdot \\ X_i^{\mathrm{t}} & else_t \cdot \end{Bmatrix} \tag{16}$$

X_i^{t+1} characterizes the novel state of the $i\ th$ zebra according to the first stage. PZ refers to pioneer zebra. PZ_j stands for $j\ th$ dimension (optimal solution). $x_{i,j}^{t+1}$ signifies $j\ th$ dimension value of the $i\ th$ zebra. r and $rand$ indicate randomly generated numbers in the interval $[0,1]$. $I \in \{1,2\}$, when $I = 2$, there is an extra change in the movement of the population.

2) DEFENCE

The next stage is the defence mechanisms of the zebra. The location of the ZOA population in the search area is upgraded utilizing defences against predator assaults. Lions are main predators of zebras. Moreover, hyenas, cheetahs, and leopards are also dangerous to zebras. After zebras meet these predators, they select the strategies of escape (Sl) or aggressive $(S2)$. During the escape approach, the zebra selects an escape path against the attack of the lion, whereas a small predator like a wild dog attacks, it and attempts to fright it by utilizing an aggressive approach. Eqs state the zebra's movement in the defense phase. (17) and (18).

$$x_{i,j}^{t+1} = \begin{cases} S1: x_{i,j}^{\tau} + R \cdot (2r - 1) \cdot \left(1 - \dfrac{r}{T_{max}}\right) \cdot x_{i,j}^{t}, & if(P_s) \\ S2: x_{i,j}^{\tau} + r \cdot (AZ_j - l \cdot x_{i,j}^{\tau})_t & else; \end{cases} \tag{17}$$

$$X_i^t = \begin{Bmatrix} X_i^{t+1}, & if(F_i^{t+1} < F_i^{\tau}); \\ X_i^{\mathrm{t}}, & else; \end{Bmatrix} \tag{18}$$

Now, X_i^{t+1} refers to $i\ th$ zebra's updated position, with $x_{i,j}^{t+1}$ representing its $j\ th$ dimension value and F_i^{t+1} being its value of the objective function. The variable t denotes the present iteration, the maximal iteration count is T and the constant value R is 0.01. $P_s$signify the likelihood of picking one of two randomly produced tactics inside the interval $[0,1]$, AZ represents the state of the attacked zebra and AZ_j is its $j\ th$ value of the dimension.

The fitness selection is the substantial factor, which influences the ZOA performance. The process of hyperparameter selection includes the solution encoded system for evaluating the efficiency of candidate solution. Here, the ZOA reflects accuracy as the main standard to project the FF. Its mathematical formulation is given below.

$$Fitness = \max(P) \tag{19}$$

$$P = \frac{TP}{TP + FP} \tag{20}$$

Here, TP suggests the positive value of true and FP indicates the positive value of false.

4. Experimental Result Analysis

In this section, the experimental validation of the WDDZOA-ELRSI technique is verified under the disaster images dataset [24]. This dataset contains 1600 images under 4 disasters. The complete details of this dataset are depicted in Table 1. Fig. 3 displays the sample images.

DOI: https://doi.org/10.54216/FPA.190117
Received: October 14, 2024 Revised: January 03, 2025 Accepted: February 02, 2025

Table 1: Details of the dataset

Disasters	No. of Images
Cyclone	400
Earthquake	400
Flood	400
Wildfire	400
Total Images	1600

Figure 3. Sample Images a) Cyclone b) Earthquake c) Flood d) Wildfire

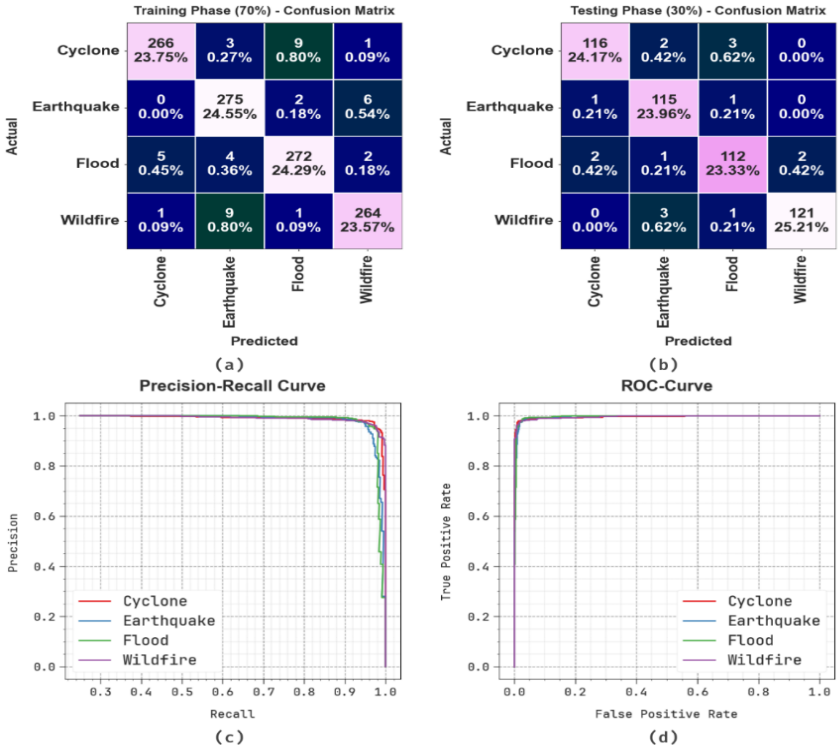

Figure 4. Classifier outcome of (a-b) 70% and 30% confusion matrix and (c-d) curves of PR and ROC

DOI: https://doi.org/10.54216/FPA.190117
Received: October 14, 2024 Revised: January 03, 2025 Accepted: February 02, 2025

Fig. 4 displays the classifier performances of the WDDZOA-ELRSI technique. Figs. 4a-4b illustrates the confusion matrices through specific classification of all classes below 70%TRAPHA and 30%TESPHA. Fig. 4c exemplifies the PR examination, which notified higher outcomes through all distinct classes. Eventually, Fig. 4d displays the ROC inspection, signifying capable solutions with high ROC values for different class labels.

The weather disaster detection of the WDDZOA-ELRSI model below 70%TRAPHA and 30%TESPHA is displayed in Table 2 and Fig. 5. The results implied that the WDDZOA-ELRSI technique suitably classified all the samples. Based on 70%TRAPHA, the WDDZOA-ELRSI method delivers typical $accu_y$ of 98.08%, $prec_n$ of 96.19%, $reca_l$ of 96.16%, $F1_{score}$of 96.17%, and MCC of 94.89%. Additionally, using 30%TESPHA, the WDDZOA-ELRSI algorithm provides typical $accu_y$ of 98.33%, $prec_n$ of 96.66%, $reca_l$ of 96.67%, $F1_{score}$of 96.65%, and MCC of 95.55%.

Table 2: Weather disaster detection of WDDZOA-ELRSI model under 70%TRAPHA and 30%TESPHA

Class Labels	$Accu_y$	$Prec_n$	$Reca_l$	$F1_{score}$	MCC
TRAPHA (70%)					
Cyclone	98.30	97.79	95.34	96.55	95.44
Earthquake	97.86	94.50	97.17	95.82	94.40
Flood	97.95	95.77	96.11	95.94	94.57
Wildfire	98.21	96.70	96.00	96.35	95.17
Average	98.08	96.19	96.16	96.17	94.89
TESPHA (30%)					
Cyclone	98.33	97.48	95.87	96.67	95.56
Earthquake	98.33	95.04	98.29	96.64	95.55
Flood	97.92	95.73	95.73	95.73	94.35
Wildfire	98.75	98.37	96.80	97.58	96.74
Average	98.33	96.66	96.67	96.65	95.55

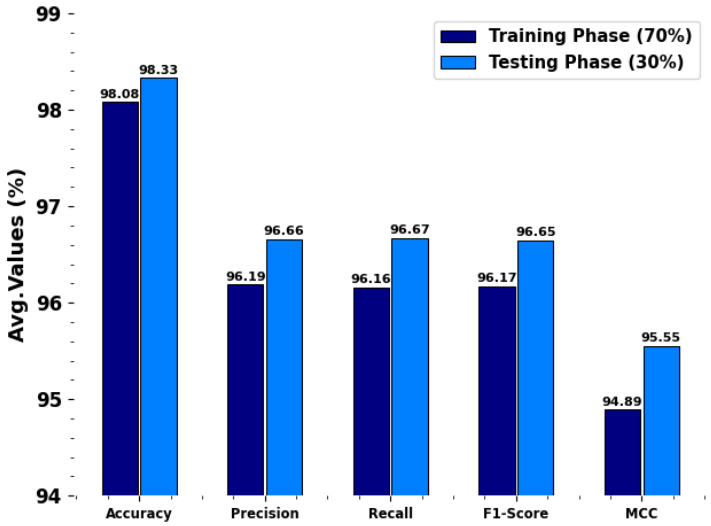

Figure 5. Average of WDDZOA-ELRSI model under 70%TRAPHA and 30%TESPHA

DOI: https://doi.org/10.54216/FPA.190117
Received: October 14, 2024 Revised: January 03, 2025 Accepted: February 02, 2025

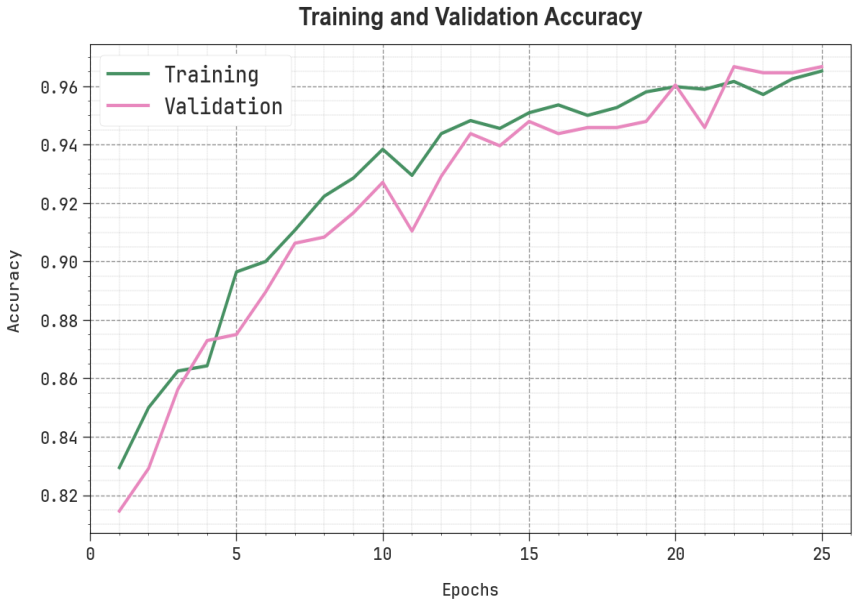

Figure 6. $Accu_y$ Curve of the WDDZOA-ELRSI model

In Fig. 6, the training (TRAN) $accu_y$ and validation (VALN) $accu_y$ performances of the WDDZOA-ELRSI technique are exemplified. The values of $accu_y$ are computed across a time of 0-25 epochs. The figure underscored that the TRAN and VALN $accu_y$ values present a cumulative propensity to notify the competency of the WDDZOA-ELRSI system through enhanced outcomes over several iterations. Furthermore, the TRAN and VALN $accu_y$ values remain close across the epochs, which notified diminished overfitting and expresses superior performance of the WDDZOA-ELRSI algorithm, which guarantees reliable calculation on unseen samples.

In Fig. 7, the TRAN loss (TRANLOS) and VALN loss (VALNLOS) graph of the WDDZOA-ELRSI method is shown. The values of loss are calculated through a time of 0-25 epochs. It is depicted that the values of TRANLOS and VALNLOS represent a declining propensity, notifying the capacity of the WDDZOA-ELRSI approach in equalizing an equilibrium between generalization and data fitting. The succeeding dilution in values of loss also assurances the maximum performance of the WDDZOA-ELRSI system and tunes the calculation results gradually.

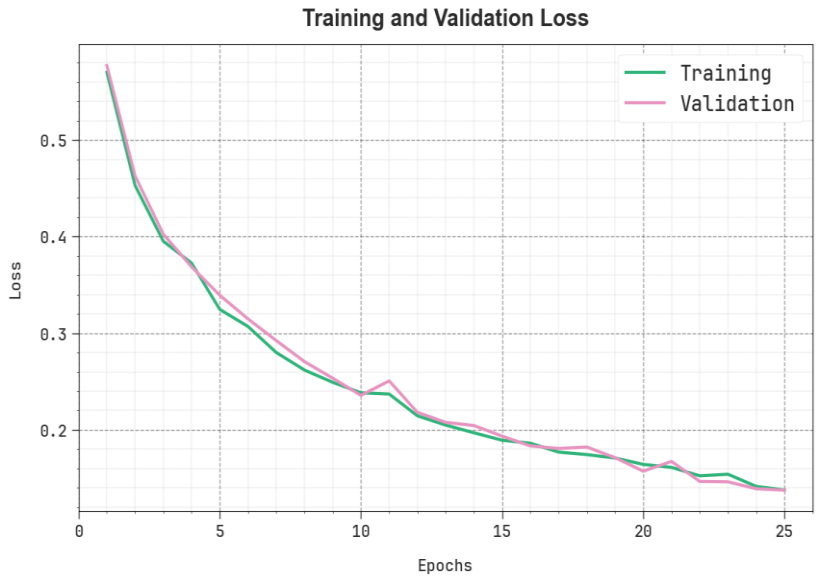

Figure 7. Loss curve of WDDZOA-ELRSI model

The comparative study of WDDZOA-ELRSI technique with existing algorithms is displayed in Table 3 and Fig. 8 [25, 26]. The model performance reported that the WDDZOA-ELRSI method outperformed greater performances.

DOI: https://doi.org/10.54216/FPA.190117
Received: October 14, 2024 Revised: January 03, 2025 Accepted: February 02, 2025

Table 3: Comparative analysis of WDDZOA-ELRSI model with existing techniques

Model	$Accu_y$	$Prec_n$	$Reca_l$	$F1_{score}$
U-Net-resnet18	95.01	92.87	95.95	89.60
DeepLab-resnet101	94.80	89.89	94.18	94.75
DeebLab-vgg11	97.60	91.82	92.50	92.54
PSO-LSTM-GAT	96.86	91.22	93.13	90.14
BERT-tiny	94.63	95.86	91.05	92.13
ALBERT-base	93.84	91.80	94.24	95.44
XtremeDistil	91.16	94.33	89.26	93.22
WDDZOA-ELRSI	98.33	96.66	96.67	96.65

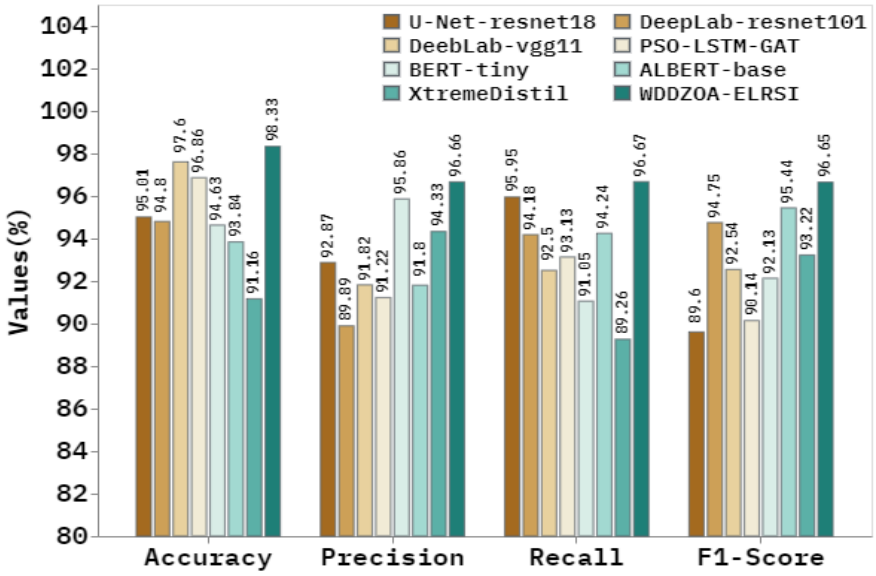

Figure 8. Comparative analysis of WDDZOA-ELRSI model with existing methods

According to $accu_y$, the WDDZOA-ELRSI system has superior $accu_y$ of 98.33% whereas the U-Net-resnet18, DeepLab-resnet101, DeebLab-vgg11, PSO-LSTM-GAT, BERT-tiny, ALBERT-base, and XtremeDistil methodologies have attained decreased $accu_y$ of 95.01%, 94.80%, 97.60%, 96.86%, 94.63%, 93.84%, and 91.16%, correspondingly. Moreover, according to $Prec_n$, the WDDZOA-ELRSI technique has maximum $Prec_n$ of 96.66% whereas the U-Net-resnet18, DeepLab-resnet101, DeebLab-vgg11, PSO-LSTM-GAT, BERT-tiny, ALBERT-base, and XtremeDistil models have reached diminish $Prec_n$ of 92.87%, 89.89%, 91.82%, 91.22%, 95.86%, 91.80%, and 94.33%, respectively. Also, according to $F1_{score}$, the WDDZOA-ELRSI algorithm has increased $F1_{score}$ of 96.65% whereas the U-Net-resnet18, DeepLab-resnet101, DeebLab-vgg11, PSO-LSTM-GAT, BERT-tiny, ALBERT-base, and XtremeDistil methods have gained minimum $F1_{score}$ of 89.60%, 94.75%, 92.54%, 90.14%, 92.13%, 95.44%, and 93.22%, respectively.

5. Conclusion

In this manuscript, we design and develop a WDDZOA-ELRSI technique. The proposed WDDZOA-ELRSI approach main intention is to improve the detection model of weather disasters using state-of-the-art DL methods. Initially, the BF method is employed in the image pre-processing stage to eliminate the unwanted noise from input data. Furthermore, the feature extraction method executes GoogleNet technique to transform raw data into a

DOI: https://doi.org/10.54216/FPA.190117
Received: October 14, 2024 Revised: January 03, 2025 Accepted: February 02, 2025

reduced set of relevant features. For the classification process, an ensemble of DL models such as CVAE, GCN, and ERNN models have been deployed. Eventually, the ZOA-based hyperparameter tuning procedure has been achieved to improve the detection outcomes of ensemble models. The simulation analysis of the WDDZOA-ELRSI system is verified on a benchmark image dataset and the outcomes were evaluated under numerous measures. The simulation outcome emphasized the enhancement of the WDDZOA-ELRSI model in the weather disaster detection process.

Funding: "This research received no external funding"

Conflicts of Interest: "The authors declare no conflict of interest."

References

[1] J. Al Qundus, K. Dabbour, S. Gupta, R. Meissonier, and A. Paschke, "Wireless sensor network for AI-based flood disaster detection," *Annals of Operations Research*, pp. 1-23, 2022.

[2] R. Dhanagopal and B. Muthukumar, "A model for low power, high speed and energy efficient early landslide detection system using IoT," *Wireless Personal Communications*, vol. 117, no. 4, pp. 2713-2728, 2021.

[3] C. Rambour, N. Audebert, E. Koeniguer, B. Le Saux, M. Crucianu, and M. Datcu, "Flood detection in time series of optical and SAR images," *The International Archives of the Photogrammetry, Remote Sensing and Spatial Information Sciences*, vol. 43, no. B2, pp. 1343-1346, 2020.

[4] J. Kim, S. H. Kim, H. W. Seo, Y. V. Wang, and Y. G. Lee, "Meteorological characteristics of fog events in Korean smart cities and machine learning based visibility estimation," *Atmospheric Research*, vol. 275, p. 106239, 2022.

[5] N. Takahashi et al., "Development of multi-parameter phased array weather radar (MP-PAWR) and early detection of torrential rainfall and tornado risk," *Journal of Disaster Research*, vol. 14, no. 2, pp. 235-247, 2019.

[6] L. Tan, J. Guo, S. Mohanarajah, and K. Zhou, "Can we detect trends in natural disaster management with artificial intelligence? A review of modeling practices," *Natural Hazards*, vol. 107, pp. 2389-2417, 2021.

[7] M. Park, Y. Jeon, J. Bak, and S. Park, "Forest-fire response system using deep-learning-based approaches with CCTV images and weather data," *IEEE Access*, vol. 10, pp. 66061-66071, 2022.

[8] A. Marathe, D. Ramanan, R. Walambe, and K. Kotecha, "Wedge: A multi-weather autonomous driving dataset built from generative vision-language models," in *Proceedings of the IEEE/CVF Conference on Computer Vision and Pattern Recognition*, pp. 3318-3327, 2023.

[9] J. Dong, K. Ota, and M. Dong, "UAV-based real-time survivor detection system in post-disaster search and rescue operations," *IEEE Journal on Miniaturization for Air and Space Systems*, vol. 2, no. 4, pp. 209-219, 2021.

[10] X. Yuan and R. Atassi, "Geological landslide disaster monitoring based on wireless network technology," *Full Length Article*, vol. 2, no. 1, pp. 21-1, 2021.

[11] R. F. Mansour and E. Alabdulkreem, "Disaster monitoring of satellite image processing using progressive image classification," *Computer Systems Science & Engineering*, vol. 44, no. 2, 2023.

[12] A. Shastry et al., "Mapping floods from remote sensing data and quantifying the effects of surface obstruction by clouds and vegetation," *Remote Sensing of Environment*, vol. 291, p. 113556, 2023.

[13] A. Sarkar et al., "SAM-VQA: Supervised attention-based visual question answering model for post-disaster damage assessment on remote sensing imagery," *IEEE Transactions on Geoscience and Remote Sensing*, vol. 61, pp. 1-16, 2023.

[14] M. Roohi, H. R. Ghafouri, and S. M. Ashrafi, "Advancing flood disaster management: leveraging deep learning and remote sensing technologies," *Acta Geophysica*, vol. 73, no. 1, pp. 557-575, 2025.

[15] A. Hamza et al., "A novel bottleneck residual and self-attention fusion-assisted architecture for land use recognition in remote sensing images," *IEEE Journal of Selected Topics in Applied Earth Observations and Remote Sensing*, 2024.

DOI: https://doi.org/10.54216/FPA.190117
Received: October 14, 2024 Revised: January 03, 2025 Accepted: February 02, 2025

[16] D. J. Paul and S. P. Janani, "Advanced weather monitoring and disaster mitigation system," in *2024 International Conference on Cognitive Robotics and Intelligent Systems (ICC-ROBINS)*, pp. 540-546, 2024.

[17] J. Ge, H. Tang, N. Yang, and Y. Hu, "Rapid identification of damaged buildings using incremental learning with transferred data from historical natural disaster cases," *ISPRS Journal of Photogrammetry and Remote Sensing*, vol. 195, pp. 105-128, 2023.

[18] S. Mekala and P. K. Singamsetty, "A hybrid approach for pancreatic cancer detection in CT scans using secretary wolf bird optimization and deep learning," *Available at SSRN*, 5134659.

[19] M. T. Ashfaq et al., "Scalable hybrid deep models for individual pharmacy cost prediction," *IEEE Access*, 2025.

[20] M. Shan et al., "Ada-GCNLSTM: An adaptive urban crime spatiotemporal prediction model," *Journal of Safety Science and Resilience*, 2025.

[21] X. Zhao, W. Fan, H. Liu, and J. Tang, "Multi-type urban crime prediction," in *Proceedings of the AAAI Conference on Artificial Intelligence*, vol. 36, no. 5, pp. 574-582, 2022.

[22] H. Alfraihi et al., "A multi-model feature fusion based transfer learning with heuristic search for copy-move video forgery detection," *Scientific Reports*, vol. 15, no. 1, p. 4738, 2025.

[23] F. A. Özbay, "An enhanced zebra optimization algorithm with multiple strategies for global optimization and feature selection problems: A hepatocellular carcinoma case study," *IEEE Access*, 2025.

[24] [Online]. Available: https://www.kaggle.com/datasets/mikolajbabula/disaster-images-dataset-cnn-model.

[25] R. Camacho, J. Aryal, and A. Rajabifard, "How do disasters disrupt the spatial growth of informal settlements? A multi-temporal remote sensing approach–The case study of Mocoa, Colombia," *Habitat International*, vol. 156, p. 103272, 2025.

[26] S. Saleem et al., "Deltran15: A deep lightweight transformer-based framework for multiclass classification of disaster posts on X," *IEEE Access*, 2024.

DOI: https://doi.org/10.54216/FPA.190117
Received: October 14, 2024 Revised: January 03, 2025 Accepted: February 02, 2025